BIOCHEMISTRY
including biophysical chemistry & molecular biology

Article

pubs.acs.org/biochemistry

Manipulating Conserved Heme Cavity Residues of Chlorite Dismutase: Effect on Structure, Redox Chemistry, and Reactivity

Stefan Hofbauer,[†] Kira Gysel,[‡] Marzia Bellei,[⊥] Andreas Hagmüller,[‡] Irene Schaffner,[†] Georg Mlynek,[‡] Julius Kostan,[‡] Katharina F. Pirker,[†] Holger Daims,[∥] Paul G. Furtmüller,[†] Gianantonio Battistuzzi,[#] Kristina Djinović-Carugo,*[,‡,§] and Christian Obinger*[,†]

[†]Department of Chemistry, Division of Biochemistry, VIBT − Vienna Institute of BioTechnology, BOKU − University of Natural Resources and Life Sciences, A-1190 Vienna, Austria

[‡]Department for Structural and Computational Biology, Max F. Perutz Laboratories, University of Vienna, A-1030 Vienna, Austria

[§]Department of Biochemistry, Faculty of Chemistry and Chemical Technology, University of Ljubljana, 1000 Ljubljana, Slovenia

[⊥]Department of Life Sciences, University of Modena and Reggio Emilia, 41125 Modena, Italy

[∥]Department of Microbiology and Ecosystem Science, Division of Microbial Ecology, University of Vienna, A-1090 Vienna, Austria

[#]Department of Chemistry and Geology, University of Modena and Reggio Emilia, 41125 Modena, Italy

Supporting Information

ABSTRACT: Chlorite dismutases (Clds) are heme *b* containing oxidoreductases that convert chlorite to chloride and molecular oxygen. In order to elucidate the role of conserved heme cavity residues in the catalysis of this reaction comprehensive mutational and biochemical analyses of Cld from "*Candidatus* Nitrospira defluvii" (NdCld) were performed. Particularly, point mutations of the cavity-forming residues R173, K141, W145, W146, and E210 were performed. The effect of manipulation in 12 single and double mutants was probed by UV−vis spectroscopy, spectroelectrochemistry, pre-steady-state and steady-state kinetics, and X-ray crystallography. Resulting biochemical data are discussed with respect to the known crystal structure of wild-type NdCld and the variants R173A and R173K as well as the structures of R173E, W145V, W145F, and the R173Q/W146Y solved in this work. The findings allow a critical analysis of the role of these heme cavity residues in the reaction mechanism of chlorite degradation that is proposed to involve hypohalous acid as transient intermediate and formation of an O═O bond. The distal R173 is shown to be important (but not fully essential) for the reaction with chlorite, and, upon addition of cyanide, it acts as a proton acceptor in the formation of the resulting low-spin complex. The proximal H-bonding network including K141-E210-H160 keeps the enzyme in its ferric ($E^{\circ\prime}$ = −113 mV) and mainly five-coordinated high-spin state and is very susceptible to perturbation.

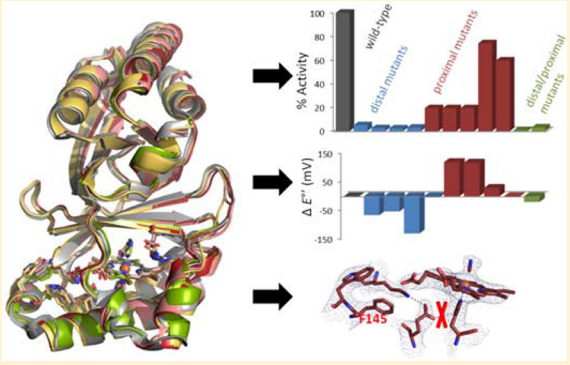

In 1996 a heme *b* containing and chlorite degrading oxidoreductase was discovered in chlorate- and perchlorate-reducing facultative anaerobic bacteria (PCRB).[1] The metalloprotein (EC 1.13.11.49) was found to degrade chlorite to chloride and molecular oxygen, and the misleading and chemically incorrect name chlorite dismutase (Cld) was assigned to it.[1] As it was initially found in PCRBs, it was attributed a role of protecting PCRBs from accumulation of harmful chlorite. In recent years, homologous proteins were found in many other bacterial and archaeal phyla. Reconstruction of the phylogeny of chlorite dismutases as well as elucidation of X-ray structures revealed the presence of two main clades of active enzymes as well as similarities in overall fold and heme cavity architecture with another relatively new family of so-called dye-decolorizing peroxidases.[2−8]

X-ray structures are available for representatives of both phylogenetically separated main Cld lineages. Three-dimensional structures of Clade 1 comprise homopentameric Clds from *Dechloromonas aromatica* (PDB codes 3QO8, 3QO9: 3.05 and 3.0 Å resolution, respectively)[5] and "*Candidatus* Nitrospira defluvii" (3NN1, 3NN2: 1.85 and 1.94 Å resolution, respectively)[6] and homohexameric Cld from *Azospira oryzae* (2VXH: 2.1 Å),[7] whereas Clade 2 Clds seem to be homodimeric proteins [Cld from *Nitrobacter winogradskyi* (3QPI: 2.1 Å)[8]]. Besides differences in oligomeric architecture, Clds of Clades 1 and 2 exhibit differences in subunit structure[5−8] as well as in conformational and thermal stability.[9] Despite these disparities in overall structure and stability, the heme binding cavity provides an almost identical environment

Received: August 1, 2013
Revised: December 23, 2013
Published: December 23, 2013

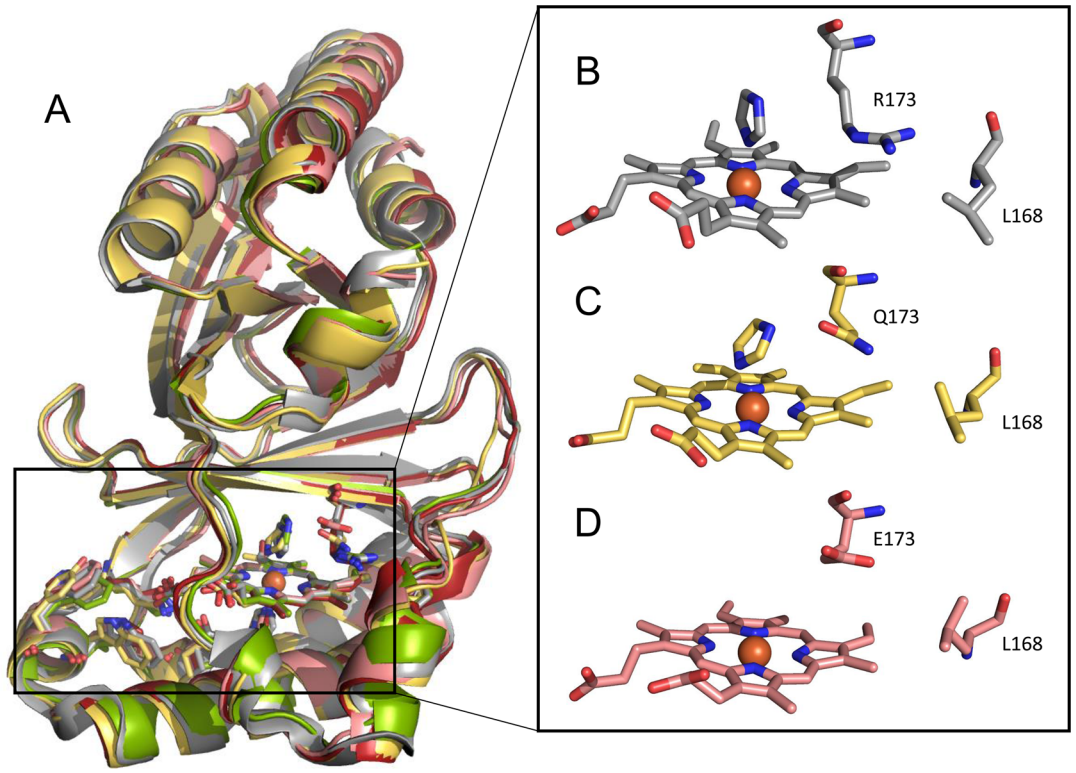

Figure 1. Overlay of subunit and distal heme architecture of NdCld wild-type and variants. (A) Cartoon representation of NdCld wild-type and the variants R173E, R173QW146Y, W145V, and W145F with the respective heme and active site residues represented as sticks. (B–D) Enlargement of the distal heme side of NdCld wild-type (B), and variants R173QW146Y (C) and R173E (D). Figures were generated using PyMOL (http://www.pymol.org/).

in Clds from both clades.[5−8] This is supported by the fact that both the high-spin and low-spin forms of Clds from *Candidatus Nitrospira defluvii* (NdCld) and *Nitrobacter winogradskyi* (NwCld) exhibit similar standard reduction potentials of the Fe(III)/Fe(II) couple[10] as well as similar chlorite degradation activity (NdCld: $k_{cat}/K_M = 6.2 \times 10^5$ M^{-1} s^{-1}; NwCld: $k_{cat}/K_M = 2.1 \times 10^6$ M^{-1} s^{-1}) .[6,8]

The prosthetic group in chlorite dismutases is heme *b*, which is proximally coordinated by a histidine (His160, NdCld numbering) that is hydrogen-bonded to a glutamate residue (E210). This couple of amino acids, together with neighboring lysine (K141) and two tryptophan residues (W145, W146), are found in all structures of functional Clds solved so far (Figure 1).[5−8] The most prominent and fully conserved amino acid residue on the distal side of functional Clds is an arginine (R173). Its side chain is flexible and is found in diverse conformations in crystal structures of Clds: either pointing away from the heme *b* iron toward the putative substrate entrance[6,8] or oriented toward the active site.[5,7] The latter conformation seems to be stabilized by anionic ligands.[6] Being the only charged residue in the distal side, R173 was proposed to participate in the chlorite degradation mechanism. Namely, R173 was suggested to be involved in substrate binding and reduction as well as in stabilization of the transient intermediate hypochlorous acid (reaction 1).[6,11]

The following redox pathway has been proposed based on a few studies.[11−14] The native ferric heme enzyme is oxidized to a transient intermediate (compound I) state, which — in analogy to conventional heme peroxidases — was suggested to be an oxoiron(IV)porphyryl radical [$Por^{\bullet+}Fe(IV)=O$] (reaction 1).[12] The reaction product hypochlorous acid must be kept close to the oxoferryl-oxygen since it serves as two-electron donor, thereby restoring the Fe(III)-state and releasing chloride and dioxygen (reaction 2). In the second half-reaction, an O–O bond is formed, a reaction so far only described in the water-splitting manganese complex of photosystem II of oxygenic phototrophic organisms[15] and in a yet uncharacterized enzyme of an anaerobic methane-oxidizing bacterium.[16]

$$PorFe(III) + [O\text{-}Cl\text{-}O]^- \rightarrow Por^{\bullet+}Fe(IV) = O\cdots[O\text{-}Cl^-] \quad (1)$$

$$Por^{\bullet+}Fe(IV) = O\cdots[O\text{-}Cl^-] \rightarrow PorFe(III) + O = O + Cl^- \quad (2)$$

Proof of reactions 1 and 2 requires the characterization of the electronic and spectral properties of the involved (transient) redox states and reaction products, the kinetics of interconversion and the role(s) of the conserved heme cavity residues in these reactions. Two Clds have been used for those studies so far, namely, chlorite dismutases from *Dechloromonas aromatica* (DaCld)[11,17] and NdCld,[6] suggesting a catalytic role for the distal arginine[6,11] and the formation of protein radical(s).[17] Notably, DaCld and NdCld show tremendous spectral differences [e.g., the Soret maximum at pH 7.0 has been reported to be at 393 nm (DaCld)[17] and 408 nm (NdCld)[10]]. Diverse spectral properties could be related to significant differences in the conformational and thermal stability of enzymes in solution,[9] since the crystal structures[5,6] show an almost identical heme cavity architecture. Six crystal structures of NdCld variants were solved successfully [see ref 6 and this work], whereas no structures of DaCld mutants are reported.[11,17]

dx.doi.org/10.1021/bi401042z | *Biochemistry* 2014, 53, 77−89

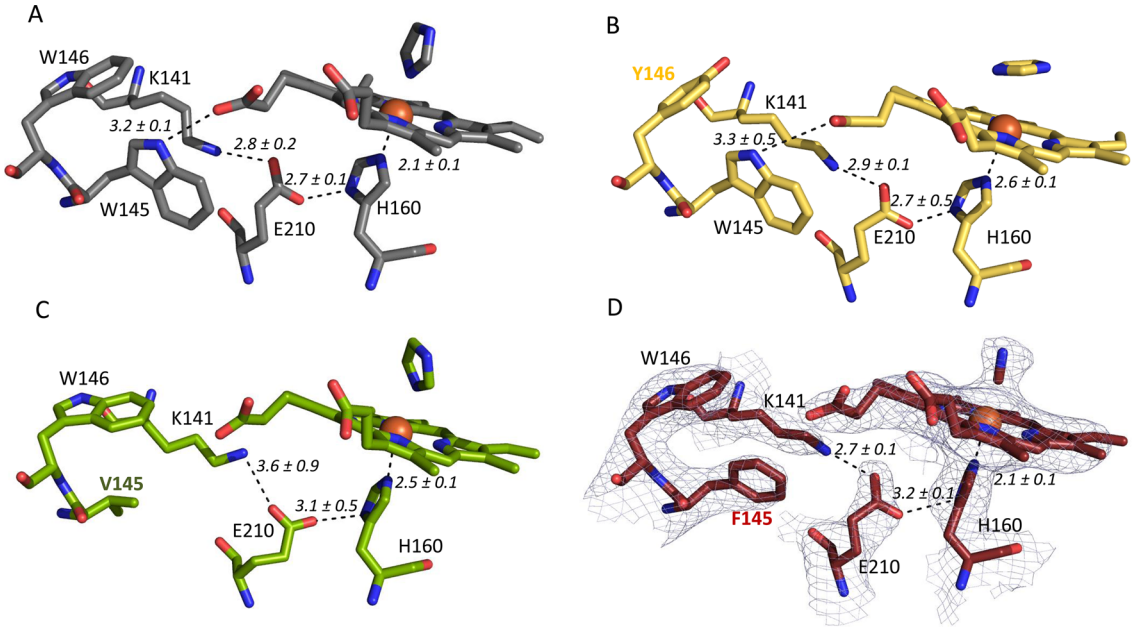

Figure 2. Architecture of the proximal heme side of wild-type NdCld (A) and the variants W146Y (B), W145V (C) and W145F together with its 2|F_o| − |F_c| electron density map countered at 1σ level (D). Figures were generated using PyMOL (http://www.pymol.org/). Putative H-bonds are shown as dotted black lines.

In this study we have analyzed the role of residues suggested to be important for the catalysis of chlorite degradation (R173, E210, K141, W145, and W146) (Figures 1 and 2), with special emphasis on the role of conserved residues on the proximal side and further evaluation of the distal arginine. The single mutants R173E, R173Q, E210A, K141E, W145F, W145V, W146Y and the double mutants W145V/W146Y, R173Q/E210A, and R173Q/W146Y were recombinantly produced in *Escherichia coli* and thoroughly biochemically characterized. Recombinant production and first characterization of distal mutants R173A and R173K were reported previously[6] and are studied more extensively in this work. In detail, the effect of mutation(s) on the UV−vis spectra, the redox properties of the Fe(III)/Fe(II) couple, the enzymatic parameters of chlorite degradation (K_M, k_{cat}, and k_{cat}/K_M) as well as the kinetics of cyanide binding were analyzed. Moreover, mutants R173E, W145V, W145F as well as R173Q/W146Y were structurally characterized using X-ray crystallography. The structures of these mutants together with already available structures of wild-type NdCld and the variants R173A and R173K[6] and the obtained biochemical/physical data allow a comprehensive structure−function analysis of this new enzyme family. The importance of R173 in the chlorite degradation reaction and formation of the Cld-cyanide complex is demonstrated and discussed as is the role of the K141-E210-H160 triad in maintenance of the heme cavity architecture and redox properties.

MATERIALS AND METHODS

Site-Directed Mutagenesis, Expression, and Purification. To obtain plasmids for expressing the NdCld variants R173A, R173K, R173E, R173Q, E210A, K141E, W145F, W145V, W146Y mutagenesis was carried out using Phusion-Flash polymerase (Finnzymes) with primers and their reverse complements listed in Supplemental Table 1, Supporting Information. The plasmid encoding the N-terminal TEV-cleavable Strep-II tagged fusion protein wild-type NdCld (without the N-terminal signal peptide) was used as template. Cloning of the wild-type NdCld plasmid was described previously.[6] To obtain plasmids for expressing the double mutated NdCld proteins R173Q/W146Y and R173Q/E210A, the plasmid of R173Q was used as a template. Similarly, for the double mutant W145V/W146Y the plasmid of W146Y was used as template (Supplemental Table 1). Total volume of mutagenesis PCR was 20 μL and a two-step thermocycle was followed (98 °C for denaturation, 72 °C for annealing and elongation). Original templates were digested with *DpnI* (Fermentas) and PCR product was transformed into *E. coli* DH5α cells (Invitrogen). Plasmid DNA was extracted using GeneJET Plasmid Miniprep Kit (Fermentas), and sequencing was performed from T7prom and T7term by LGC Genomics to confirm successful site-directed mutagenesis.

Recombinant wild-type NdCld was expressed in *E. coli* Tuner (DE3) cells (Merck/Novagen, Darmstadt, Germany) and purified via a StrepTrap HP 5 mL (GE Healthcare) column as it was described previously.[9] All mutants were expressed and purified using the same protocol as for the wild-type protein.

Crystallization, Data Collection, and Processing. The NdCld variants W145V, R173Q/W146Y were concentrated to 10 mg/mL and stored in buffer (20 mM HEPES, pH 7.4, 2% glycerol) and crystallized in conditions containing high ammonium sulfate and low pH ranges from 3.5 to 4.5 (derived from condition 13 of JCSG+ commercial screen, Qiagen), which is similar to crystallization conditions of the wild-type NdCld.[6] For cryoprotection, the crystal was soaked stepwise in the mother liquor containing increasing concentrations (10%) of ethylene glycol up to final 50% (v/v). The mutant R173E was crystallized in 0.1 M sodium acetate, pH 4, and 40% (v/v) ethylene glycol (condition 2 from the Cryol+II screen, Emerald Biosciences), which already served as a cryoprotectant. W145F with and without cyanide was crystallized in 0.7−0.8 M ammonium citrate dibasic in 100 mM sodium acetate buffers pH 4.4−4.5 and 30% (v/v) ethylene glycol.

Diffraction data were collected either in-house on a Bruker Microstar (Bruker AXS Inc.) rotating anode at 1.54 Å

dx.doi.org/10.1021/bi401042z | *Biochemistry* 2014, 53, 77−89

Table 1. Data Collection and Refinement Statistics[a]

	NdCld R173E	NdCld W146Y R173Q	NdCld W145F +CN	NdCld W145F	NdCld W145V
PDB code	4m05	4m09	4m06	4m07	4m08
wavelength (Å)	0.976	0.872	0.872	0.872	1.54
resolution range (Å)	44.22−2.28 (2.36−2.28)	44.38−2.45 (2.54−2.45)	43.45−2.6 (2.69−2.60)	43.55−2.5 (2.59−2.50)	63.15−2.80 (2.90−2.80)
space group	*C* 1 2 1	*C* 1 2 1	*C* 1 2 1	*C* 1 2 1	*P* 32 2 1
unit cell	136.47 112.39 119.25 90 117.8 90	138.1 114.98 118.87 90 118.1 90	136.21 113.42 118.84 90 117.9 90	138.29 112.61 120.32 90 118.5 90	145.83 145.83 137.225 90 90 120
total reflections	707036 (40837)	190696 (17024)	340749 (17213)	148231 (5141)	1490427 (89611)
unique reflections	72249 (6981)	59228 (5551)	47172 (3833)	48975 (2676)	41940 (4097)
multiplicity	9.8 (5.8)	3.2 (3.1)	7.2 (4.5)	3.0 (1.9)	35.5 (21.9)
completeness (%)	99.60 (96.78)	98.29 (92.58)	96.00 (78.55)	87.29 (48.08)	99.92 (99.39)
mean $I\sigma(I)$	5.30 (0.23)	5.69 (0.39)	10.01 (0.38)	12.64 (0.23)	23.34 (2.08)
Wilson *B*-factor	30.0	33.7	59.8	52.9	49.8
R-merge	0.371 (6.865)	0.1964 (3.48)	0.1423 (3.495)	0.06243 (3.033)	0.1957 (1.657)
R-meas	0.3915	0.2366	0.1532	0.07519	0.1984
$CC_{1/2}$	0.993 (0.129)	0.99 (0.231)	0.998 (0.149)	0.999 (0.148)	0.998 (0.817)
CC*	0.998 (0.478)	0.998 (0.613)	0.999 (0.509)	1 (0.508)	0.999 (0.948)
R-work	0.2680 (0.4283)	0.2774 (0.4470)	0.2111 (0.4901)	0.2050 (0.4511)	0.2205 (0.2922)
R-free	0.3201 (0.4562)	0.3325 (0.4377)	0.2584 (0.4906)	0.2535 (0.4491)	0.2798 (0.4065)
resolution $I/\sigma(I) > 2$	2.93	2.99	2.93	2.93	2.80
R-free @ $I/\sigma(I) > 2$	0.2710	0.2894	0.2310	0.2293	0.2798
number of atoms	19584	10015	19422	19567	10082
macromolecules	9588	9544	9543	9524	9560
ligands	227	306	239	291	390
water	133	165	5	47	114
protein residues	1190	1190	1190	1188	1190
RMS (bonds)	0.009	0.003	0.005	0.008	0.004
RMS (angles)	1.160	0.751	0.944	1.101	0.783
Ramachandran favored (%)	97	96	97	95	98
Ramachandran outliers (%)	0	0.26	0	0.26	0
clash-score	4.52	6.83	3.50	3.48	5.82
average *B*-factor	73.4	68.1	92.0	94.3	62.0
macromolecules	74.1	68.9	92.5	94.8	62.4
ligands	56.5	56.0	74.9	83.1	60.6
solvent	48.4	45.5	65.8	68.7	37.1

[a]Statistics for highest-resolution shell are shown in parentheses.

wavelength or at several ESRF beamlines (ID23-1, BM14-U). Integration and scaling was done with XDS and XSCALE[18] for data collected at ESRF beamlines, while diffraction data in-house was integrated and scaled with the software package Proteum2 (Bruker AXS Inc.). Data collection statistics are summarized in Table 1.

Phasing, Model Building, Refinement, and Validation of the Structures. All structures were solved by molecular replacement using the program MOLREP.[19] Chain A from the wild-type NdCld structure (3NN1)[6] was used as search template.

Model building and refinement steps were performed with PHENIX suite[20] and COOT.[21] The overall structure quality was judged with the web server MOLPROBITY.[22] Refinement statistics are summarized in Table 1.

In assessing the data quality and establishing the resolution cutoff we relied on novel, recently published criteria based on correlation coefficient $CC_{1/2}$.[23] We then performed a controlled paired-refinement,[23,24] where the starting model was refined using the same refinement protocol against both a full data set and a truncated version (to 2.85−2.95 Å) of the full data set. The resulting two models were then compared in terms of *R* values (R_{work}, R_{free}) to judge which model was better (Supplemental Table 2, Supporting Information). In all cases apart from W145F CN, the paired-refinement showed superior model quality and lower R factors when high-resolution diffraction cutoff was used. In case of W145F CN we opted for the high-resolution cutoff as well, despite slightly higher *R*-factor because of good model quality and lower overall B-factors.

Structure factors and coordinates are deposited in the Protein Data Bank: R173E (entry code 4M05), W145V (4M08), W145F (4M07), cyanide complex of W145F (4M06), and R173QW146Y (4M09), respectively.

UV−vis Spectroscopy. Spectra of wild-type NdCld and mutants were recorded between 250 and 800 nm with an Agilent 8453 diode array spectrophotometer (Hewlett-Packard). Protein concentration varied between 10 and 25 μM in 50 mM phosphate buffer, pH 7.0 . The enzymes were reduced with 10 mM sodium dithionite from a freshly prepared stock solution.

Steady-State Kinetics. Chlorite dismutase mediated degradation of chlorite was monitored by measuring the release of O_2 using a Clark-type oxygen electrode (Oxygraph Plus; Hansatech Instruments, Norfolk, United Kingdom) inserted into a stirred water bath kept at 30 °C. The electrode was

dx.doi.org/10.1021/bi401042z | *Biochemistry* 2014, 53, 77−89

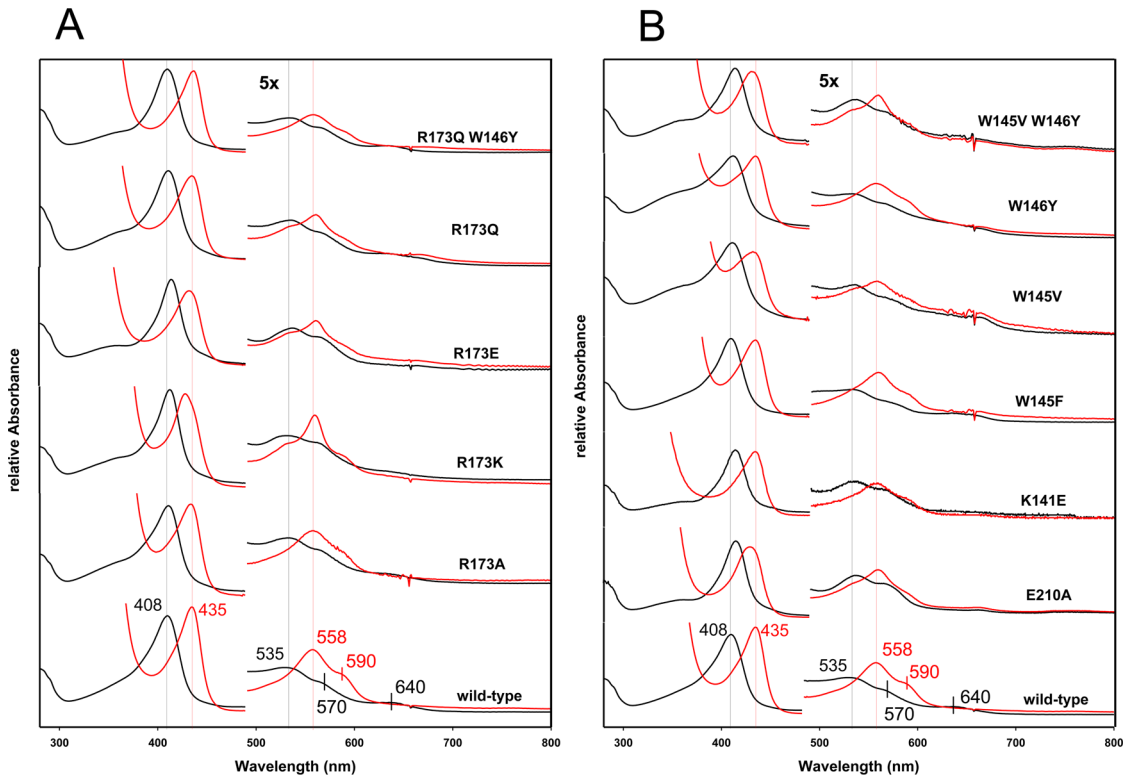

Figure 3. UV−vis spectra of NdCld wild-type and mutant proteins in oxidized (ferric) and reduced (ferrous) states at pH 7.0. (A) UV−vis spectra of distal side variants including the double mutant R173Q/W146Y. (B) UV−vis spectra of proximal side variants. Spectra of ferric proteins are depicted in black, and those of ferrous forms are in red.

equilibrated to 100% O_2 saturation by bubbling O_2 to the reaction mixture for at least 10 min and for 0% saturation by bubbling with N_2 for at least 15 min to derive an offset and calibration factor. Reactions were carried out in O_2-free 50 mM phosphate buffer, pH 7.0, with 10 μM to 2 mM $NaClO_2$ added from a stock made in the same buffer. Reactions were started by addition of 20 nM of wild-type NdCld or 200−400 nM of mutants. With increasing chlorite concentrations, irreversible inactivation of the enzyme occurred, as was evident with inspection of individual time traces. Therefore it was important to use only the initial linear phase for rate computation of the Michaelis−Menten parameters. Molecular oxygen production rates (μM O_2 s^{-1}) were obtained from initial linear time traces (<10% substrate consumed) and plotted against chlorite concentrations.

Transient-State Kinetics. The experiments were carried out with a stopped-flow apparatus (model SX-18MV, Applied Photophysics) equipped for both conventional and sequential measurements. The optical quartz cell with a path length of 10 mm had a volume of 20 μL. The fastest time for mixing two solutions and recording the first data point was 1.3 ms. All measurements were performed at 25 °C. For studies on cyanide binding to ferric wild-type NdCld and the mutants, the conventional stopped-flow mode was used, and the decrease of the absorbance at the respective Soret maximum was monitored. In a typical experiment, one syringe contained 0.5 μM enzyme in 50 mM phosphate buffer, pH 7.0, and the second syringe contained at least a 5-fold excess of cyanide in the same buffer; in detail cyanide concentrations ranged from 2.5 μM to 5000 μM. A minimum of four measurements were performed for each ligand concentration. The apparent second-order rate constants, k_{on}, were obtained from the slope of a plot of k_{obs} versus cyanide concentration. Routinely, cyanide binding was also monitored by using the diode array detector (Applied Photophysics), which allowed the synthesis of artificial sets of time-dependent spectra as well as spectral analysis of enzyme intermediates.

Spectroelectrochemistry. All experiments were carried out in a homemade optical transparent thin-layer spectroelectrochemical (OTTLE) cell.[10,25,26] The three-electrode configuration consisted of a gold minigrid working electrode (Buckbee-Mears, Chicago, IL), a homemade Ag/AgCl/KCl_{sat} microreference electrode, separated from the working solution by a Vycor set, and a platinum wire as the counter electrode.[10,24] The reference electrode was calibrated against a saturated calomel (Hg_2Cl_2) electrode before each set of measurements. All potentials are referenced to the standard hydrogen electrode (SHE, +242 mV).

Potentials were applied across the OTTLE cell with an Amel model 2053 potentiostat/galvanostat. Constant temperature was maintained by a circulating water bath, and the OTTLE cell temperature was monitored with a Cu-costan microthermocouple. UV−vis spectra were recorded using a Varian Cary C50 spectrophotometer. The OTTLE cell was flushed with Argon gas to establish an oxygen-free environment in the cell.

Spectroelectrochemical experiments were performed using 650 μL samples containing 4−6 μM of wild-type or mutant NdCld in 150 mM phosphate buffer, pH 7.0, plus 100 mM NaCl, in the presence of various mediators: methyl viologen, lumiflavine-3-acetate, methylene blue, phenazine methosulfate, and indigo carmine. The concentration of each mediator in the cell was 4.6 μM, except for methyl viologen (230 μM). Nernst plots consisted of at least five points and were invariably linear with a slope consistent with a one-electron reduction process

dx.doi.org/10.1021/bi401042z | Biochemistry 2014, 53, 77−89

(n-values of wild-type and mutant NdClds varied between between 1.0 and 1.4).

Variable temperature experiments for NdCld as well as for selected mutants were carried out using a nonisothermal cell configuration over a temperature range from 10 to 35 °C.[24] The temperature of the reference electrode and the counter electrode was kept constant, whereas that of the working electrode was varied. Parametrization of enthalpic and entropic components was possible by calculating $\Delta S_{rc}^{\circ\prime}$ from the slope of the plot $E^{\circ\prime}$ versus temperature; $\Delta H_{rc}^{\circ\prime}$ could be obtained from the Gibbs−Helmholtz equation, thus from the slope of the plot $E^{\circ\prime}/T$ versus $1/T$.[25,26]

RESULTS

Recombinant Production and Spectral Characterization of NdCld Variants. Native and mutated NdClds were expressed in *E. coli*. With the exception of the double mutant R173Q/E210A, the heme occupancy in all variants was higher than 85% meaning that the purity numbers (Reinheitszahlen) $A_{Soret,max}/A_{280\ nm}$ varied between 1.7 and 2.2 (Supplemental Table 3, Supporting Information).

Figure 3 shows the UV−vis spectra of oxidized (ferric) and reduced (ferrous) states of wild-type NdCld and all mutants investigated in this work. The spectroscopic properties of ferric wild-type NdCld are indicative of a dominating high-spin (HS) heme b[10] with a Soret maximum at 408 nm, Q bands at 535 and 570 nm, and a charge-transfer (CT) band at 640 nm (Figure 3 and Supplemental Table 3). Charge-transfer bands are typical for high-spin heme proteins and are located within the range 610−650 nm, with five-coordinated (5c) HS being typically ≥640 nm and six-coordinated (6c) HS around 630 nm.

With the exception of the double mutant R173Q/E210A, the Soret maxima of all variants were red-shifted (408−414 nm) compared to the native protein. The distal mutants R173K and R173E as well as the proximal variants E210A and K141E had their Soret maximum at 414 nm and did not show any absorbance in the CT region, indicating that the heme group had pronounced low-spin character.

Upon addition of cyanide to these ferric proteins, the corresponding low-spin variants were formed having the Soret maxima around 420 nm (see below), that is, red-shifted by 9−12 nm compared to the corresponding high-spin state. Concomitantly, the CT absorbance disappeared. Upon reduction by dithionite, most of the variants showed similar high-spin ferrous spectra with Soret maxima between 432 and 435 nm and Q bands at 558−560 and 590 nm (Figure 3 and Supplemental Table 3). Spectra of ferrous R173K, E210A, and the double mutant R173Q/E210A exhibited blue-shifted Soret maxima at 428, 430, and 424 nm respectively indicating the presence of ferrous low-spin species.

X-ray structures of NdCld R173E, W145V, W145F, and R173Q/W146Y. The X-ray structures of wild-type chlorite dismutase from "*Candidatus* Nitrospira defluvii" as well as the two variants R173A and R173K have been published recently.[6] In order to enable a comprehensive analysis of the structural and functional role of conserved active site residues in Clds the X-ray structures of additional variants (R173E, W145V, W145F, R173QW146Y) were determined (Figure 1). Data were collected and crystal structures were refined for R173E, W145V, and R173QW146Y. In both W145V and R173QW146Y, an imidazole served as the sixth ligand of the heme b. The mutant W145F was crystallized without and with cyanide bound to the heme iron.

W145V crystallized in the hexagonal space group $P3_221$, whereas W145F, R173E, and R173QW146Y crystallized in the monoclinic space group $C2$ (Table 1). Each subunit of wild-type NdCld and its mutants is composed of two topologically equivalent ferredoxin-like domains, as was described in detail by Kostan et al.[6] The overall structure of the subunits of the mutants does not change compared to the wild-type protein, with r.m.s.d. deviations between equivalent C_α atoms ranging from 0.310 Å for mutant W145F+CN to 0.518 Å for the R173Q/W146Y double mutant (Figure 1A).

The five subunits in the wild-type and mutant proteins are arranged in a ring-like fashion around a central channel. The active site of NdCld is located in a cavity of the C-terminal ferredoxin-like domain with heme b embedded in a defined hydrophobic environment. On the distal heme side, the only residue able to provide a positive charge, or to shift toward the active site in the presence of an anionic ligand, is Arg173. In wild-type NdCld arginine 173 was shown to be oriented away from the heme iron and points toward the putative substrate entrance (Figure 1B).[6] In the structure of the mutant R173K, the lysine side chain points into the heme cavity and forms a hydrogen bond with a trapped sulfate anion.[6] Figure 1C,D depicts the structures of R173Q and R173E with imidazole and acetate (present in crystallization solution) bound at the distal site of the heme iron. The side chain of the negatively charged glutamic residue in R173E is oriented away from the heme iron, similar to what is observed for R173 in wild-type NdCld. In the mutant protein, the side chain of L168 shifts toward E173, filling in this way the cavity occupied in the wild-type NdCld by the guanidinium group of R173 (Figure 1).

Figure 2A depicts the proximal H-bonding network of wild-type NdCld including H160-E210-K141. The H-bond between the proximal histidine and E210 (2.7 Å) keeps the heme ligand in the imidazolate state. Only small changes were observed when W146 was exchanged by tyrosine except an increase in the bond length between H160 and the heme iron (Figure 2B). The proximal NdCld variants W145V and W145F were designed with the rationale to probe the role of this fully conserved aromatic residue in redox catalysis. One of the heme propionate carboxylate groups interacts with the NE1 atom of Trp145 which might indicate the possibility of forming a radical site at this position during enzyme turnover.[5] Upon its replacement by a smaller valine, a cavity is formed (Figure 2C), and the neighboring W146 (oriented orthogonally to W145 in the wild-type Clds) is tilted by about 20° compared to the wild-type structure. Additionally, the H-bonding network within the conserved amino acid triad K141, E210, and H160 on the proximal side is weakened in the absence of W145 (Figure 2), with both K141 and E210 forming alternative H-bonds with solvent molecules. Additionally, in the mutant W145V the H-bond between E210 and H160 appears 0.6 Å longer compared to the wild-type protein (2.7 Å) (Figure 2C).

As expected, upon replacement of the W145 residue by a bulky phenylalanine, the architecture of the heme cavity is similar to wild-type NdCld, with one important difference. In the mutant W145F the H-bond between E210 and H160 is broken (length: 3.2 Å) (Figure 2D). We did not succeed in obtaining the crystal structures of NdCld K141E and E210A.

The double mutant R173Q/W146Y was designed to mimic chlorite dismutase-like proteins that differ in their active site composition from the canonical Clds, such as the Cld-like protein from *Listeria monocytogenes*. In this variant, only minor structural effects were observed (Figure 1), for example, a

dx.doi.org/10.1021/bi401042z | *Biochemistry* 2014, 53, 77−89

Table 2. Kinetics of Chlorite Degradation and Cyanide Binding of Wild-Type "*Candidatus* Nitrospira defluvii" and a Series of Distal and Proximal Heme Cavity Mutants: (A) Steady-State Kinetic Parameters of Chlorite Degradation Following the Release of O_2 Polarographically and (B) Pre-Steady-State Kinetic Parameters for Cyanide Binding (k_{on}) and Dissociation (k_{off}). The Dissociation Constant K_D Was Calculated from the Ratio k_{off}/k_{on}

	(A)			(B)			
	K_M (μM)	k_{cat} (s^{-1})	k_{cat}/K_M (M^{-1} s^{-1})	k_{on} (M^{-1} s^{-1})	k_{off} (s^{-1})	K_D (μM)	
wild-type	69 ± 6	43.0	6.2×10^5	2.6×10^6	9.3	3.6	(6)
Arg173Ala	90 ± 9	2.8	3.1×10^4	3.4×10^3	0.5	145.8	(6)
Arg173Lys	898 ± 138	14.0	1.5×10^4	1.6×10^3	0.3	185.2	(6)
Arg173Glu	195 ± 27	2.7	1.4×10^4	73	0.3	3,874	this study
Arg173Gln	130 ± 7	2.3	1.8×10^4	2.3×10^3	0.5	216.4	this study
Glu210Ala	382 ± 15	46.7	1.2×10^5	40	0.7	17,300	this study
Lys141Glu	70 ± 19	32.5	4.6×10^5	50	1.9	38,800	this study
Trp145Phe	172 ± 10	20.0	1.2×10^5	1.9×10^6	2.9	1.5	this study
Trp145Val	103 ± 11	12.0	1.2×10^5	2.7×10^5	3.9	14.6	this study
Trp146Tyr	87 ± 8	32.0	3.7×10^5	1.1×10^6	9.7	9.2	this study
Trp145Val Trp146Tyr	106 ± 23	22.0	2.9×10^5	5.3×10^5	4.6	8.7	this study
Arg173Gln Glu210Ala	184 ± 36	0.9	4.6×10^3	no binding			this study
Arg173Gln Trp146Tyr	205 ± 18	4.0	1.9×10^4	1.5×10^3	0.1	84.4	this study

change in the orientation of L168 (as in R173E, see above), while Y146 is found in the same position as W146 in wild-type NdCld.

Enzymatic Activity of NdCld Mutants with Chlorite. In order to probe the effect of exchange of active site residues of "*Candidatus* Nitrospira defluvii" on the degradation of chlorite, the release of O_2 at pH 7.0 was followed polarographically (Table 2). As long as the substrate concentration was below 1 mM (in order to avoid Cld inactivation), a typical Michaelis–Menten behavior was seen, and data could be fitted best with a single rectangular hyperbola function (Supplemental Figure 1, Supporting Information). Wild-type NdCld has a catalytic efficiency k_{cat}/K_M of 6.2×10^5 M^{-1} s^{-1} and a K_M of 69 μM. Exchange of Arg173 decreased the catalytic efficiency [wild-type (100%) > R173A (5%) > R173Q (2.9%) > R173K (2.4%) > R173E (2.3%)] and increased the Michaelis constant [wild-type (100%) < R173A (130%) < R173Q (188%) < R173E (283%) < R173K (1301%)]. It was interesting to see that (i) R173E is still able to degrade ClO_2^- to some extent (its k_{cat} is still ~6.3% of the wild-type value) and that (ii) substitution of a R173 by another basic amino acid (lysine) increased the K_M by a factor of 13 (Table 2).

From the proximal variants, W146Y exhibited an enzymatic activity very similar to the wild-type protein. Tryptophan 146 is not directly involved in the proximal H-bonding network that stabilizes heme ligation by H160. By contrast, exchange of the direct H-bonding partner (E210) of the proximal histidine by alanine leads to a decrease of the catalytic efficiency by 87% compared to the wild-type protein. The significant increase in the K_M value of the variant E210A (382 μM) compared to the wild-type enzyme reflects a more than 5-fold decrease in chlorite binding at the distal heme cavity. By comparison, the effect of disruption of the hydrogen bond between lysine 141 and glutamate 210 in the mutant K141E was relatively small (Table 2). The two variants having the fully conserved proximal tryptophan 145 exchanged (W145F and W145V) exhibit k_{cat}/K_M values of about 20% of the wild-type enzyme.

The effects of mutations in the three double variants on the enzymatic activity seemed to be additive. The double mutant R173Q/E210A has the lowest catalytic efficiency and a turnover number smaller than 1 s^{-1}. The double mutant of NdCld R173Q/W146Y, which mimics the heme cavity of the chlorite dismutase-like protein from *Listeria monocytogenes*, still has a catalytic efficiency of 1.9×10^4 M^{-1} s^{-1}.

Kinetics of Formation of the Low-Spin Cyanide Complex of Cld Variants. Cyanide is a low-spin ligand that is often used to probe the accessibility of the active site of heme proteins. Manipulation of the (distal) heme cavity architecture is often reflected by changes in both binding rates as well as in the strength of binding of cyanide to the ferric heme iron. Figure 4A shows a representative spectral conversion when ferric mutant W145F was mixed with cyanide monitored with the stopped-flow apparatus. The corresponding time trace followed at 408 nm is depicted in the inset. Cyanide converts the high-spin ($S = 5/2$) ferric iron state to the low-spin ($S = 1/2$) ferric state, thereby shifting the Soret maximum from 408 to 420 nm with a clear isosbestic point at 414 nm. The time traces could be fitted best by a double-exponential equation [obtaining pseudo-first-order rate constants $k_{obs(1)}$ and $k_{obs(2)}$; Figure 4A] with $k_{obs(1)}$ being responsible for more than 90% of the decrease in absorbance and $k_{obs(2)}$ showing no dependence on concentration of cyanide (Figure 4B, inset) as was reported for wild-type NdCld.[6] As a consequence, the apparent second-order rate (k_{on}) constant for cyanide binding was calculated from the slope of the linear plot of $k_{obs(1)}$ versus cyanide concentration (Figure 4B). In contrast, cyanide binding to distal arginine mutants R173Q, R173Q/W146Y, and R173E was monophasic, and k_{obs} was obtained by single exponential fits, which is in agreement with cyanide binding studies of R173A and R173K.[6]

Obtained data suggest that manipulation of proximal W145 and W146 only slightly affected cyanide binding at the distal side (Table 2). By contrast, in both E210A and K141E mutants cyanide binding was extremely slow, and the dissociation constant increased by 4 orders of magnitude (Table 2). Since in (i) all four variants the H-bond between E210 and H160 is extended or broken, and (ii) cyanide binding of W145F (with broken H-bond) is similar to wild-type NdCld, these

dx.doi.org/10.1021/bi401042z | *Biochemistry* 2014, 53, 77–89

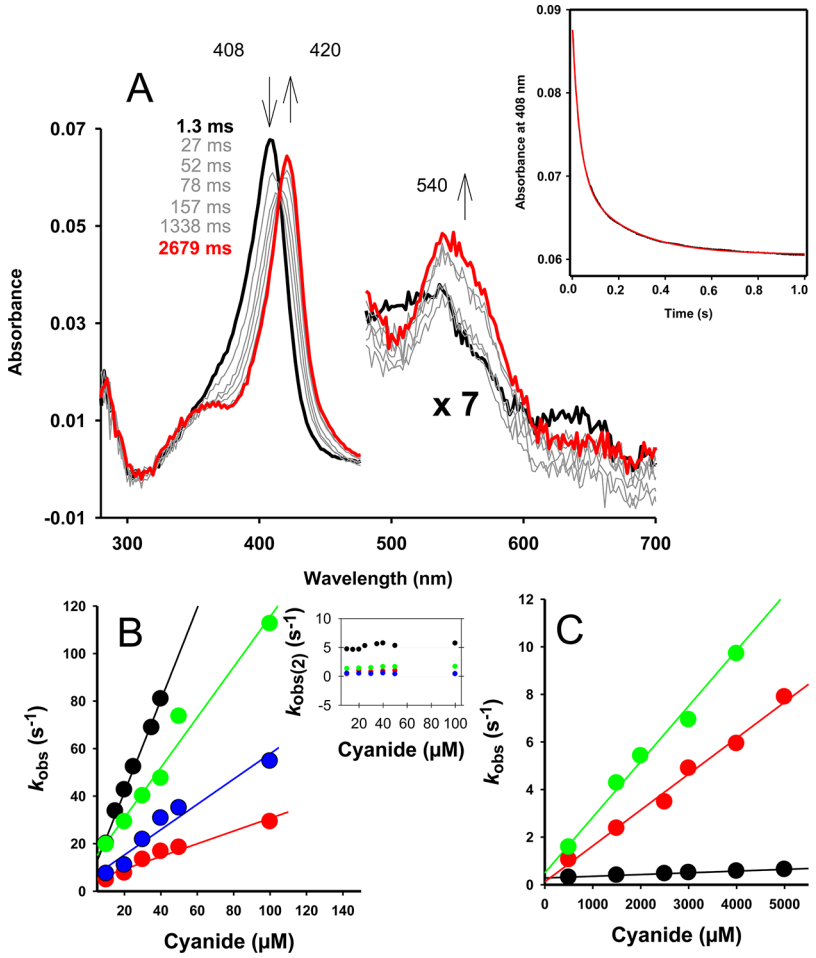

Figure 4. Kinetics of cyanide binding to ferric high-spin NdCld Trp145Phe followed by stopped-flow spectroscopy. (A) Spectral changes upon reaction of 0.5 μM NdCld W145F with 10 μM cyanide measured in the conventional stopped-flow mode. The first spectrum shows native high-spin NdCld W145F (Soret band at 408 nm), the second spectrum was recorded 1.3 ms after mixing. Subsequent spectra show the formation of the low-spin cyanide complex (absorbance maximum 420 nm). Arrows indicate changes of absorbance with time. Conditions: 50 mM phosphate buffer, pH 7.0, and 25 °C. The inset shows a typical time trace at 408 nm with double exponential fit (0.7 μM NdCld W145F and 15 μM cyanide). Linear dependence of $k_{obs(1)}$ and $k_{obs(2)}$ (inset) from the cyanide concentration is shown in (B) for NdCld W145F (black), NdCld W145V (red), NdCld W146Y (green), NdCld W145V/W146Y (blue), as well as in (C) for NdCld R173E (black), NdCld R173Q (red), and NdCld R173Q/W146Y (green).

differences in cyanide complex formation cannot be related with the imidazolate character of the proximal histidine. It is reasonable to assume that the performed mutations at E210 and K141 led to significant changes of both the proximal and distal heme cavity architecture, which is also reflected by the high low-spin character of these variants that hinders cyanide binding.

As already previously reported,[6] cyanide binding to wild-type NdCld and the variants R173A and R173K were monophasic, and exchange of R173 showed a significantly decreased bimolecular rate constant as well as increased K_D values [= k_{off}/k_{on}, with k_{off} representing the intercepts of the linear plots in Figure 4B,C]. Upon exchanging the positively charged arginine 173 with the negatively charged glutamate, cyanide binding is even more impeded, whereas the binding kinetics of NdCld R173Q and R173Q/W146Y is comparable with R173A and R173K (Figure 3C and Table 2). In any case, Table 2 demonstrates that the impact of exchange of arginine 173 on the catalytic efficiency of chlorite degradation is significantly smaller than on the binding of the low-spin ligand cyanide.

Spectroelectrochemical Analyses. Figure 5 depicts a representative family of spectra of ferric wild-type NdCld (Figure 5A) and variants R173E (Figure 5B), R173K (Figure 4C), and W145F (Figure 5D) at different applied potentials in the OTTLE cell. The pentameric wild-type metalloprotein is directly reduced to its ferrous form with absorption maxima at 435 and 560 nm with a clear isosbestic point at 420 nm. The calculated reduction potential for the Fe(III)/Fe(II) couple, determined from the corresponding Nernst plot (inset to Figure 5A), was calculated to be at −0.113 ± 0.001 V at 25 °C and pH 7.0.[10] The slope of the Nernst plot indicates that a single electron is exchanged.

Table 3 summarizes the $E^{\circ\prime}$ values obtained for the various Cld variants. The mutant R173Q exhibited a wild-type-like reduction potential, whereas exchange of arginine 173 by negatively charged glutamate shifted the reduction potential by about 120 mV to more negative values. Additionally, mutation of arginine 173 to small and uncharged alanine lowered $E^{\circ\prime}$ by 66 mV. In both R173E and R173A variants, the ferric state has been stabilized due to deletion of the positively charged guanidinium group. In all these distal mutant proteins, the

dx.doi.org/10.1021/bi401042z | Biochemistry 2014, 53, 77−89

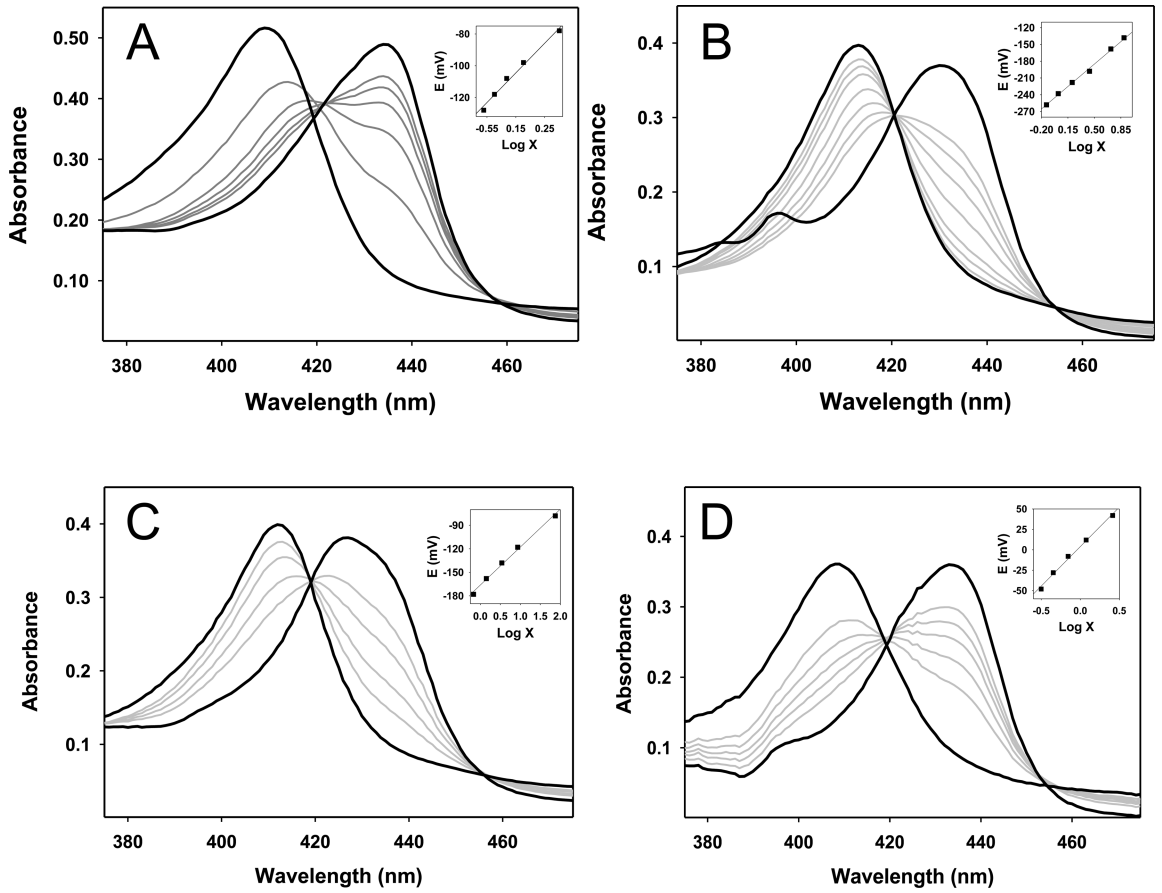

Figure 5. Spectroelectrochemistry of NdCld variants. Representative electronic spectra of (A) wild-type chlorite dismutase from "*Candidatus* Nitrospira defluvii", (B) NdCld R173E, (C) NdCld R173K, and (D) NdCld W145F at various potentials at 25 °C and pH 7.0. The insets depict the corresponding Nernst plots, were X represents the ratio $(A_{\lambda red}{}^{max} - A_{\lambda red})/(A_{\lambda ox}{}^{max} - A_{\lambda ox})$. For wild-type NdCld: λ_{ox} = 410 nm and λ_{red} = 435 nm. For the variants, the corresponding Soret maxima of the ferric and ferrous states are summarized in Table 3.

Table 3. Standard Reduction Potentials of Wild-Type Chlorite Dismutase from "*Candidatus* Nitrospira defluvii" and Distal and Proximal Heme Cavity Variants Obtained from Spectroelectrochemical Measurements[a]

	$E^{\circ\prime}$ (mV)	$\Delta H_{rc}^{\circ\prime}$ (kJ mol^{-1})	$\Delta S_{rc}^{\circ\prime}$ (J mol^{-1} K^{-1})	$-\Delta H_{rc}^{\circ\prime}/F$ (mV)	$T\Delta S_{rc}^{\circ\prime}/F$ (mV)	$-FE^{\circ\prime}$ ($=\Delta H^{\circ\prime}{}_{rc(int)}$) (kJ mol^{-1})
wild-type	−113 ± 1.0	+29 ± 6	+63 ± 20	−305 ± 60	+194 ± 60	+10.9 ± 0.1
Arg173Ala	−179 ± 1.5	ND[c]	ND	ND	ND	
Arg173Lys	−166 ± 2.0	+2 ± 32	+6 ± 31	−16 ± 304	+19 ± 114	+16.0 ± 0.2
Arg173Glu	−243 ± 1.7	ND	ND	ND	ND	ND
Arg173Gln	−117 ± 1.0	ND	ND	ND	ND	ND
Glu210Ala	*b*					
Lys141Glu	+6 ± 2.0	ND	ND	ND	ND	ND
Trp145Phe	+4 ± 1.4	+17 ± 14	+65 ± 47	−181 ± 142	+201 ± 147	−0.4 ± 0.1
Trp145Val	−84 ± 2.1	ND	ND	ND	ND	ND
Trp146Tyr	−115 ± 1.7	ND	ND	ND	ND	ND
Trp145Val	*b*					
Trp146Tyr						
Arg173Gln	*b*					
Glu210Ala						
Arg173Gln	−133 ± 0.4	ND	ND	ND	ND	ND
Trp146Tyr						

[a]In addition, for wild-type Cld and the variants R173K and W145F the enthalpic and entropic contribution to the reduction reaction has been calculated. [b]Obtained data are not reliable due to formation of the Fe−O_2 adduct. [c]ND, not determined.

maximum of the Soret band of the ferrous form was at 435 nm and no clear shoulder at 424 nm was observed, indicating no O_2 binding to the ferrous state.

At first sight, it was surprising that exchange of arginine 173 by positively charged lysine also shifts the standard reduction potential to a more negative value compared to wild-type

dx.doi.org/10.1021/bi401042z | *Biochemistry* 2014, 53, 77−89

NdCld. However, this nicely reflects the pronounced low-spin character of this variant (see Discussion).

The proximal heme cavity variants W146Y showed a wild-type like redox behavior suggesting very limiting reorganization of H160 and E210. The $E^{\circ\prime}$ value of the mutant W145V was slightly more positive ($\Delta E^{\circ\prime}$ = +29 mV) compared to wild-type NdCld. Compared to the reorganization of the proximal H-bonding pattern observed in the X-ray structure of W145V (see above), this effect is small. Exchange of tryptophan 145 by valine disrupts the H-bond between the heme propionate and the NE1 of the mutated tryptophan residue (which should lower $E^{\circ\prime}$, since the negative charge of the propionate group increases upon the disappearance of the H-bond, in which it acts as H-bond acceptor). Additionally, this mutation promotes a reorientation of the side chains of K141 and E210, resulting in a weakening of the H-bond between H160 and E210 (which should decrease the anionic character of the proximal His and increase $E^{\circ\prime}$) as seen in the X-ray structure. Most probably both effects partly compensate in W145V.

Although the overall X-ray structure of W145F was wild-type-like, one significant difference concerns the breaking of the H-bond between the proximal histidine and E210. This was nicely reflected by the measured reduction potential for the Fe(III)/Fe(II) couple, which was much more positive ($\Delta E^{\circ\prime}$ = +117 mV) compared to the wild-type enzyme. In the X-ray structure additionally a limited rearrangement of K141 is seen. Similarly, exchange of lysine 141 by glutamate increased the reduction potential by 119 mV. The effect cannot be of electrostatic origin, since in this variant K141 was replaced by a negative residue. More likely also this mutation has disrupted the interaction between E210 and H160. Thus, weakening of the H-bonding network within the triad K141-E210-H160 and especially breaking of the H-bond between E210 and H160 leads to complete loss of the imidazolate character of H160 and significantly increases the reduction potential of the Fe(III)/Fe(II) couple.

It was not possible to obtain reliable $E^{\circ\prime}$ values for the E210A as well as the double mutants W145V/W146Y and R173Q/E210A, since the corresponding ferrous states easily bound dioxygen thus not allowing exact determination of concentrations of pure ferrous forms in the equilibria. Interestingly, $E^{\circ\prime}$ of the double mutant R173Q/W146Y of NdCld (−133 mV) is slightly more negative than $E^{\circ\prime}$ the wild-type protein and of the corresponding single mutants, indicating that the effect of the two point mutations on $E^{\circ\prime}$ is not additive. This variant resembles the residues of the heme cavity of a chlorite dismutase-like protein from *Listeria monocytogenes* (Table 3).

To gain a deeper insight into the mechanism of $E^{\circ\prime}$ modulation of wild-type NdCld and the variants R173K and W145F, the temperature dependence of the reduction potential was investigated (Figure 6). This allows parametrization of the corresponding enthalpic ($\Delta H^{\circ\prime}{}_{rc}$) and entropic ($\Delta S^{\circ\prime}{}_{rc}$) components of the reduction reaction.[25,26] Fe(III) reduction enthalpy and entropy for wild-type NdCld and for its R173K and W145F mutants are invariantly positive (Table 3). Therefore, in all proteins the reduction potential is the result of two opposing contributions: an enthalpic term, which disfavors Fe(III) reduction, and an entropic contribution, which instead favors Fe(III) reduction. Thus, the enthalpy and entropy changes partially compensate. The negative $E^{\circ\prime}$ of native Cld is due to the large enthalpic term (+29 kJ mol^{-1}), which overcomes the smaller, yet relevant, entropic contribution (+63 J K^{-1} mol^{-1}). The significant enthalpic stabilization

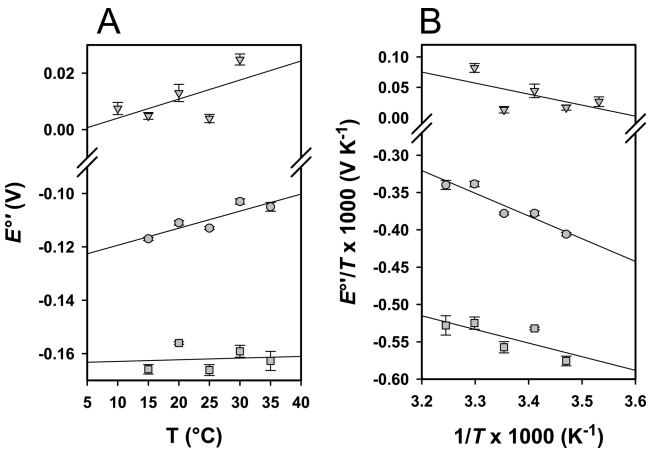

Figure 6. Reduction thermodynamics of wild-type NdCld and the variants R173K and W145F. (A) Temperature dependence of the reduction potential and (B) $E^{\circ\prime}/T$ versus $1/T$ plots for wild-type NdCld (circles), NdCld R173K (squares) and NdCld W145F (diamonds). The slope of the plot yields the $\Delta S^{\circ\prime}_{rc}/F$ (A) and $-\Delta H^{\circ\prime}_{rc}/F$ (B) values, respectively. Solid lines are least-squares fits to the data points. All experiments were carried out in 150 mM phosphate buffer, pH 7.0, containing 100 mM NaCl.

of the ferric enzyme is consistent with the anionic character conferred to the proximal histidine by the H-bond network formed with the E210 and K141. Compared to plant heme peroxidases, this effect seems to be partially offset by mutation-induced deletion of the hydrogen bond connecting one of the heme propionates with the ring of the native tryptophan and by the increased hydrophobicity of heme pocket.[25] The positive reduction entropy of native Cld is consistent with reduction-induced solvent reorganization effects in the catalytic site, since the decreased electrostatic interaction of the metal ion in its reduced form with the water molecules in the cavity should lead to a decrease in ordering.[25,26] Further contributions to the positive $\Delta S^{\circ\prime}{}_{rc}$ value could arise from a reduction-induced increase of the flexibility of the side chain of R173.

The relevant increase in the reduction potential of the Fe(III)/Fe(II) couple induced by the W145F mutation [$\Delta E^{\circ\prime}$ (mutant − wild-type) = +117 mV] has a fully enthalpic origin. In fact, replacement of the native tryptophan residue with a phenylalanine significantly reduces $\Delta H^{\circ\prime}_{rc}$, but does not modify $\Delta S^{\circ\prime}_{rc}$. This is consistent with the structural effects of the present mutation, which are limited to the proximal heme site and cause the breaking of the H-bond between H160 and E210, thereby decreasing the anionic character of the latter.

Surprisingly, replacement of R173 with a lysine deeply alters the reduction thermodynamics of the Fe(III)/Fe(II) couple. In fact the $E^{\circ\prime}$ of the R173K mutant does not show any pronounced temperature dependence (please note in Table 3 the big errors, which are a consequence of the very small impact of temperature on $E^{\circ\prime}$). This behavior again reflects the pronounced low-spin character of the mutant R173K (see above), which diminishes the reduction induced reorganization within the heme site.[25,26]

DISCUSSION

Chlorite dismutases constitute a novel heme enzyme family with a structurally unique active site and peculiar enzymatic properties. Being first described in perchlorate-respiring bacteria[1] that actually produce chlorite as metabolic inter-

dx.doi.org/10.1021/bi401042z | *Biochemistry* 2014, 53, 77−89

mediate, it has been found that other bacterial groups such as nitrite-oxidizing bacteria and cyanobacteria also encode this enzyme, and the chlorite-degrading activity of Clds from nitrite oxidizers was demonstrated.[6,8−10] As these organisms are not known PCRB, and it appears to be rather unlikely that chlorite is the main *in vivo* substrate of their Clds. This raises the question about the physiological role of functional Clds in these organisms and the nature of the oxidant and electron donor that catalyzes reactions 1 and 2 in these organisms. In order to address these challenging questions and identify candidate substrates other than chlorite, it is important to first understand the impact of active site residues on the well-established chlorite degradation activity. This was the aim of this study.

Three papers that report on mutational analyses of Cld functionality have been published so far using DaCld (chlorite dismutase from perchlorate-respiring *Dechloromonas aromatica*[11,17]) and NdCld (Cld from nitrite-oxidizing "*Candidatus* Nitrospira defluvii"[6]) as model proteins. It was interesting to see that DaCld and NdCld, although having the active site residues at almost identical positions, exhibit significant differences in spectral properties and conformational stability.[6,9−11,17] As the conformational and thermal stability of NdCld is high[9] and its mutants can readily be structurally elucidated by X-ray diffraction,[6] we focused on the *Nitrospira* protein as model chlorite dismutase in this work.

In all known functional and highly efficient Clds arginine 173 is fully conserved and represents the only charged amino acid in the distal heme cavity and a role in the ClO_2^- degradation activity has been postulated.[7] It has been proposed to bind the anionic oxidant chlorite [pK_a (chlorous acid, $HClO_2$) = 1.97[27]] (reaction 1) as well as to keep the proposed anionic intermediate hypochlorite [pK_a (hypochlorous acid, HClO) = 7.53[28]] in the reaction sphere. In the presence of the guanidinium group the anionic conjugate base, that is, hypochlorite, dominates (reaction 2). Conformational flexibility of R173 as suggested by inspection of the available X-ray structures[5−8] would be compatible with this role. It was interesting to see that despite exchange of R173 by small hydrophobic alanine (R173A), neutral glutamine (R173Q), positively charged lysine (R173K), and negatively charged glutamate (R173E) the respective mutants still exhibited chlorite degradation activity with relatively similar catalytic efficiencies between 2.2 and 5% of the wild-type activity at pH 7.0. More insightful is the inspection of the steady-state turnover number, k_{cat}, and the Michaelis constant, K_M. With 14 s^{-1} R173K had still 32.5% of the wild-type turnover, followed by R173A (6.5%), R173E (6.3%), and R173Q (5.4%). By contrast, the K_M value of R173K was the highest (898 μM) followed by R173E (195 μM), R173Q (130 μM), R173A (90 μM), and the wild-type protein (69 μM). If the conserved arginine residue is critical for binding and stabilizing anionic substrates and intermediates, it seems peculiar that the positively charged lysine in the mutant R173K had an even lower affinity for chlorite than R173E. However, the spectral properties of both ferric and ferrous R173K mutant (Table 1) as well as the redox data (Table 3) suggest the existence of mainly low-spin ferric heme in R173K. A low-spin heme was also detected in the R183K mutant of DaCld.[11] The X-ray structure shows that the lysine side chain points into the heme cavity to a water molecule that coordinates the Fe(III).[6] Additionally, the lysine forms a hydrogen bond with a trapped sulfate ion from the cryo-solution.[6] The low-spin character of R173K could derive from the deprotonation of the coordinating water in close proximity to two positively charged species, that is, Fe(III) and the positively charged lysine side chain. This would be consistent with the lower reduction potential of the Fe(III)/Fe(II) couple compared to the native enzyme ($\Delta E^{\circ\prime}$ = −53 mV), as well as its nearly independence from temperature ($\Delta S^{\circ\prime}_{rc}$ close to 0 J K^{-1} mol^{-1}). Existence of a low-spin complex in R173K is also reflected by a cyanide binding rate that is 3 orders of magnitude lower and a cyanide complex dissociation constant that is 50-times higher than in wild-type NdCld (Table 2).

In the crystal structure of R173E (Figure 1), the side chain points away from the heme iron. The ferric and ferrous UV−vis spectra suggest a noticeable low-spin portion in R173E. Despite the presence of the carboxylate group, the mutant was still active and its K_M value for chlorite was only increased by a factor of 2.8. By contrast, it dramatically decreased the rate of cyanide binding as well as the stability of the resulting low-spin complex (Table 2). If R173 is exchanged by a neutral side chain, k_{cat} is decreased by a factor of about 20 (R173A, R173Q), but K_M is increased only by a factor of 1.3 (R173A) and 1.9 (R173Q). Again, this decrease in chlorite degradation activity and affinity for the anionic substrate is modest compared to the decrease in the rate of cyanide binding as well as the stability of the resulting cyanide complex.

These data suggest that the distal arginine is important for chlorite binding and reduction but not fully essential for reaction 1. Even in its absence chlorite can bind and react with the ferric enzyme. The impact of exchange of Arg173 was significantly more pronounced when the binding of cyanide was studied. At pH 7 cyanide is protonated (pK_a of HCN is 9.2) and R173 is unprotonated (pK_a of 6.5) as was demonstrated recently.[29] Arginine 173 must therefore act as proton acceptor before cyanide can bind to the Lewis acid Fe(III). Thus, R173 promotes the deprotonation reaction as well as stabilization of the resulting cyanide complex (Table 2). Binding to and oxidation of the enzyme by chlorite (pK_a = 1.97) does not need the presence of a proton acceptor, but the arginine may support the attraction of the anionic substrate to the heme cavity as well as contribute to the stabilization of the initial Fe(III)-ClO_2^- complex. It is not as essential as is the distal histidine in heme peroxidases that must deprotonate hydrogen peroxide before Compound 0 formation (i.e., Fe(III)-O-O-H complex) can occur. Most probably R173 is more important in reaction 2 for keeping hypochlorite in the reaction sphere for redox reaction with compound I. Chlorite dismutases are inactivated during degradation of chlorite, but the mechanism is unknown. It will be interesting to answer this question in the near future using the R173 mutants designed in this work.

The proximal heme cavity of functional chlorite dismutases is characterized by a conserved H-bonding network including H160-E210-K141. Its disruption significantly alters the redox properties of the heme iron as well as the ligand binding behavior at the distal side. In both E210A and K141E, cyanide binding was almost completely impaired, and in the latter variant the reduction potential was more positive than in the native enzyme. Pronounced binding to molecular oxygen of the ferrous form of E210A in the spectroelectrochemical experiments also suggests some reorganization at the distal heme cavity. In wild-type NdCld, the proximal histidine has some imidazolate character due to its H-bond to E210. Upon exchange of E210 or neighboring K141, this noncovalent bond is disrupted, H160 becomes neutral, and the electron density at the heme iron is decreased. Simultaneously, the low-spin

dx.doi.org/10.1021/bi401042z | *Biochemistry* 2014, 53, 77−89

character of the respective proteins increases (Figure 3 and Supplemental Table 3). Again, as was already observed with the R173 variants, the impact of these structural changes on the chlorite degradation capacity was much smaller compared to the impact on the formation of the Cld-cyanide complex.

Generally, the proximal H-bonding network in Clds seems to be very labile and can easily be disrupted. While the mutant W146Y showed wild-type-like biochemical and physical properties, exchange of tryptophan 145 by phenylalanine significantly increased the $E^{\circ\prime}$ value of the Fe(III)/Fe(II) couple. This can be explained by the X-ray structure of W145F that shows a complete break of the H-bond between E210 and H160 thereby decreasing the electron density at the heme iron. Thus, the proximal heme cavity architecture in chlorite dismutases is very susceptible to perturbances. This could also be the reason for the observed differences between NdCld[10] and DaCld.[17] Whereas the crystal structures[5,6] show almost identical active sites, the biophysical properties are very different. The reported Soret maximum of ferric DaCld at 393 nm might reflect disruption of the interaction between the heme iron and the proximal histidine. This assumption is also supported by recent findings with proximal mutants of DaCld[17] where the variant W155F (corresponding to W145F in NdCld) showed dramatic differences compared to wild-type DaCld including loss of the characteristic pentameric oligomerization state, secondary structure as well as of the prosthetic group. The fact that also proximal mutants of NdCld could be crystallized (whereas crystallization of DaCld variants failed[17]) suggests that recombinant NdCld is the more suitable model Cld for future mechanistic studies.

■ ASSOCIATED CONTENT

Supporting Information

Supplemental Table 1 (primers used for site-directed mutagenesis of NdCld), Supplemental Table 2 (Controlled paired-refinement statistics), Supplemental Table 3 (UV−vis spectral signatures of wild-type and mutated chlorite dismutases), and Supplemental Figure 1 (Monitoring of dioxygen release by wild-type and mutated chlorite dismutase mediated chlorite degradation). This material is available free of charge via the Internet at http://pubs.acs.org.

Accession Codes

Atomic coordinates and structure factors have been deposited in the RSCB Protein Data Bank: 4M05, 4M06, 4M07, 4M08, 4M09.

■ AUTHOR INFORMATION

Corresponding Authors

*(C.O.) Phone: +43-1-47654-6073, fax: +43-1-47654-6050, e-mail: christian.obinger@boku.ac.at.

*(K.D.-C.) Phone: +43-1-4277-52203, e-mail: kristina.djinovic@univie.ac.at.

Funding

This project was supported by the Austrian Science Foundation, FWF [Doctoral program BioToP − Molecular Technology of Proteins (W1224) and the Projects P25270 and P22276]. G.M. and J.K. were supported by the Federal Ministry of Economy, Family and Youth through initiative "Laura Bassi Centres of Expertise", funding Center of Optimized Structural Studies (Project Number 253275).

Notes

The authors declare no competing financial interest.

■ ABBREVIATIONS

Cld, chlorite dismutase; NdCld, chlorite dismutase from "*Candidatus* Nitrospira defluvii"; NwCld, chlorite dismutase from *Nitrobacter winigradskyi*; DaCld, chlorite dismutase from *Dechloromonas aromatica*; $E^{\circ\prime}$, standard reduction potential; $\Delta H^{\circ\prime}_{rc}$, enthalpy change for the reaction center upon reduction of the ferric protein; $\Delta S^{\circ\prime}_{rc}$, entropy change for the reaction center upon reduction of the ferric protein; SHE, standard hydrogen electrode

■ REFERENCES

(1) van Ginkel, C. G., Rikken, G. B., Kroon, A. G. M., and Kengen, S. W. M. (1996) Purification and characterization of chlorite dismutase: a novel oxygen-generating enzyme. *Arch. Microbiol. 166*, 321−326.

(2) Maixner, F., Wagner, M., Lucker, S., Pelletier, E., Schmitz-Esser, S., Hace, K., Spieck, E., Konrat, R., Le Paslier, D., and Daims, H. (2008) Environmental genomics reveals functional chlorite dismutase in the nitrite-oxidizing bacterium Candidatus "Nitrospira defluvii". *Environ. Microbiol. 10*, 3043−3053.

(3) Sugano, Y. (2009) DyP-type peroxidases comprise a novel heme peroxidase family. *Cell. Mol. Life Sci. 66*, 1387−1403.

(4) Goblirsch, B., Kurker, R. C., Streit, B. R., Wilmot, C. M., and DuBois, J. L. (2011) Chlorite dismutases, DyPs and EfeB: 3 microbial heme enzyme families comprise the CDE structural superfamily. *J. Mol. Biol. 408*, 379−398.

(5) Goblirsch, B. R., Streit, B. R., DuBois, J. L., and Wilmot, C. M. (2010) Structural features promoting dioxygen production by *Dechloromonas aromatica* chlorite dismutase. *J. Biol. Inorg. Chem. 15*, 879−888.

(6) Kostan, J., Sjoeblom, B., Maixner, F., Mlynek, G., Furtmüller, P. G., Obinger, C., Wagner, M., Daims, H., and Djinovic-Carugo, K. (2010) Structural and functional analysis of the chlorite dismutase from the nitrite-oxidizing bacterium *Candidatus* "Nitrospira defluvii": identification of a catalytically important amino acid residue. *J. Struct. Biol. 172*, 331−342.

(7) de Geus, D. C., Thomassen, E. A. J., Hagedoorn, P.-L., Pannu, N. S., van Duijn, E., and Abrahams, J. P. (2009) Crystal structure of chlorite dismutase, a detoxifying enzyme producing molecular oxygen. *J. Mol. Biol. 387*, 192−206.

(8) Mlynek, G., Sjöblom, B., Kostan, J., Füreder, S., Maixner, F., Gysel, K., Furtmüller, P. G., Obinger, C., Wagner, M., Daims, H., and Djinović-Carugo, K. (2011) Unexpected diversity of chlorite dismutases: a catalytically efficient dimeric enzyme from *Nitrobacter winogradskyi*. *J. Bacteriol. 193*, 2408−2417.

(9) Hofbauer, S., Gysel, K., Mlynek, G., Kostan, J., Hagmüller, A., Daims, H., Furtmüller, P. G., Djinovic-Carugo, K., and Obinger, C. (2012) Impact of subunit and oligomeric structure on the thermal and conformational stability of chlorite dismutases. *Biochim. Biophys. Acta 1824*, 1031−1038.

(10) Hofbauer, S., Bellei, M., Sündermann, A., Pirker, K. F., Hagmüller, A., Mlynek, G., Kostan, J., Daims, H., Furtmüller, P. G., Djinovic-Carugo, K., Oostenbrink, C., Battistuzzi, G., and Obinger, C. (2012) Redox thermodynamics of high-spin and low-spin forms of chlorite dismutases with diverse subunit and oligomeric structures. *Biochemistry 51*, 9501−9512.

(11) Blanc, B., Mayfield, J. A., McDonald, C. A., Lukat-Rodgers, G. S., Rodgers, K. R., and Dubois, J. L. (2012) Understanding how the distal environment directs reactivity in chlorite dismutase: spectroscopy and reactivity of Arg183 mutants. *Biochemistry 51*, 1895−1910.

(12) Hagedoorn, P. L., de Geus, D. C., and Hagen, W. R. (2002) Spectroscopic characterization and ligand-binding properties of chlorite dismutase from the chlorate respiring bacterial strain GR-1. *Eur. J. Biochem. 269*, 4905−4911.

(13) Lee, A. Q., Streit, B. R., Zdilla, M. J., Abu-Omar, M. M., and Dubois, J. L. (2008) Mechanism of and exquisite selectivity for O-O bond formation by the heme dependent chlorite dismutase. *Proc. Natl. Acad. U.S.A. 105*, 15654−15659.

(14) Streit, B. R., and DuBois, J. L. (2008) Chemical and steady-state analysis of a heterologously expressed heme dependent chlorite dismutase. *Biochemistry 47*, 5271−5280.
(15) Vinyard, D. J., Ananyev, G. M., and Dismukes, G. C. (2013) Photosystem II: The Reaction Center of Oxygenic Photosynthesis. *Annu. Rev. Biochem. 82*, 577−606.
(16) Ettwig, K. F., Butler, M. K., Le Paslier, D., Pelletier, E., Mangenot, S., Kuypers, M. M. M., Schreiber, F., Dutilh, B. E., Zedelius, J., de Beer, D., Gloerich, J., Wessels, H. J. C. T., van Alen, T., Luesken, F., Wu, M. L., van de Pas-Schoonen, K. T., Op den Camp, H. J. M., Janssen-Megens, E. M., Francoijs, K.-J., Stunnenberg, H., Weissenbach, J., Jetten, M. S. M., and Strous, M. (2010) Nitrite-driven anaerobic methane oxidation by oxygenic bacteria. *Nature 464*, 543−548.
(17) Blanc, B., Rodgers, K. R., Lukat-Rodgers, G. S., and DuBois, J. L. (2013) Understanding the roles of strictly conserved tryptophan residues in O_2 producing chlorite dismutases. *Dalton Trans. 42*, 3156−31.
(18) Kabsch, W. (2010) XDS. *Acta Crystallogr., Sect. D: Biol. Crystallogr. 66*, 125−132.
(19) Vagin, A., and Teplyakov, A. (1997) MOLREP: an Automated Program for Molecular Replacement. *Appl. Cryst. 30*, 1022−1025.
(20) Adams, P. D., Afonine, P. V., Bunkóczi, G., Chen, V. B., Davis, I. W., Echols, N., Headd, J. J., Hung, L. W., Kapral, G. J., Grosse-Kunstleve, R. W., McCoy, A. J., Moriarty, N. W., Oeffner, R., Read, R. J., Richardson, D. C., Richardson, J. S., Terwilliger, T. C., and Zwart, P. H. (2010) PHENIX: a comprehensive Python-based system for macromolecular structure solution. *Acta Crystallogr., Sect. D: Biol. Crystallogr. 66*, 213−221.
(21) Emsley, P., and Cowtan, K. (2004) Coot: model-building tools for molecular graphics. *Acta Crystallogr., Sect. D: Biol. Crystallogr. 60*, 2126−2133.
(22) Davis, I. W., Murray, L. W., Richardson, J. S., and Richardson, D. C. (2004) MOLPROBITY: structure validation and all-atom contact analysis for nucleic acids and their complexes. *Nucleic Acids Res. 32*, 615−619.
(23) Karplus, P. A., and Diederichs, K. (2012) Linking crystallographic model and data quality. *Science 336*, 1030−1033.
(24) Diederichs, K., and Karplus, P. A. (2013) Better models by discarding data? *Acta Crystallogr., Sect. D: Biol. Crystallogr. 69*, 1215−1222.
(25) Battistuzzi, G., Bellei, M., Bortolotti, C. A., and Sola, M. (2010) Redox properties of heme peroxidases. *Arch. Biochem. Biophys. 500*, 21−36.
(26) Battistuzzi, G., Borsari, M., Ranieri, A., and Sola, M. (2002) Redox thermodynamics of the Fe(III/Fe(II) couple in horseradish peroxidase and its cyanide complex. *J. Am. Chem. Soc. 124*, 26−27.
(27) Holleman, A. F., and Wiberg, N. (2007) *Lehrbuch der Anorganischen Chemie*, Vol. *102*, Berlin.
(28) Harris, D. C. (2009) *Exploring Chemical Analysis*, 4th ed., p 538.
(29) Streit, B. R., Blanc, B., Lukat-Rodgers, G. S., Rodgers, K. R., and DuBois, J. L. (2010) How active-site protonation state influences the reactivity and ligation of the heme in chlorite dismutase. *J. Am. Chem. Soc. 132*, 5711−5724.